RESEARCH ARTICLE

INTERNATIONAL RESEARCH JOURNAL OF MULTIDISCIPLINARY TECHNOVATION

Asian Research Association

DOI: 10.54392/irjmt2656

Evaluation of Structural, Optical, Morphological and Colloidal Stability of NiO Nanoparticles Synthesized Through Green Method

K. Leninbarathi [a, *], O. Anand [b], S. Sathiyaraj [b], Aysha E. Shamaki [c], Alaa F. Abd El-Rehim [c], Ch. Srinivas [d], Vinayakprasanna N. Hegde [e], R.T. Karunakaran [a, *]

[a] Department of Physics, Government Arts College, Udumalpet, Tamil Nadu, India

[b] Department of Chemistry, Sri Ramakrishna Mission Vidyalaya College of Arts and Science, Coimbatore 641020, Tamil Nadu, India

[c] Physics Department, Faculty of Science, King Khalid University, AlQura'a, Abha, P.O. Box 960, Saudi Arabia.

[d] JNTU-Kakinada Research Centre, Nanomaterials and Nanomagnetism Research Laboratory, Department of Physics, Sasi Institute of Technology & Engineering, Tadepalligudem 534 101, Andhra Pradesh, India.

[e] Department of Physics, Vidyavardhaka College of Engineering, Mysuru-570002, Karnataka, India.

* Corresponding Author Email: physicsleninbarathik@gmail.com

DOI: https://doi.org/10.54392/irjmt2656

Received: 09-04-2026; Revised: 13-08-2026; Accepted: 20-08-2026; Published: 09-09-2026

Abstract: NiO nanoparticles have been produced by an eco-friendly combustion method utilizing water-based extracts from several parts of the Eichhornia crassipes plant, specifically the root, stem and leaf. Nickel nitrate hexahydrate and urea (fuel) are taken as precursors while plant extracts operated as natural stabilizers and reducing agents. We used a lot of different analytical tools to make sure that the nanoparticles we made were fully characterized. These tools included zeta potential analysis, field emission scanning electron microscopy (FESEM), photoluminescence (PL), X-ray diffraction (XRD) and Fourier transform infrared spectroscopy (FTIR). The XRD analysis confirmed that the NiO nanoparticles have a single-phase cubic structure with higher crystalline nature. The average crystallite sizes of the samples are in the range of 13 to 17 nm. The vibrational analysis of NiO nanoparticles revealed the presence of Ni-O stretching vibrations between 400 to 600 cm^{-1}. The optical band gap values are found to be in between 3.40 and 3.37 eV. The photoluminescence spectra showed too much ultraviolet and violet light, which was explained by intrinsic transitions and defect states, including oxygen vacancies. FE-SEM micrographs revealed that most of the nanoparticles are spherical and coalesced together in different ways depending on the plant extract employed. Tests of zeta potential showed that the colloids were pretty stable. This was especially true for the NiO nanoparticles that came from the stem. The results reveal that extracts from Eichhornia crassipes can be utilized to generate NiO nanoparticles with optical and structural properties that can be changed. The present analysis showed that the NiO nanoparticles are useful for photocatalysis, sensors, optoelectronics and energy devices.

Keywords: NiO Nanoparticles, Eichhornia Crassipes, Green Synthesis, Physico-Chemical Properties

1. Introduction

Nanotechnology has become a central platform for developing materials whose properties can be deliberately tuned through control of composition, crystallite size, morphology, surface chemistry, and defect structure. Metal-oxide nanoparticles are particularly important because these parameters can modify optical absorption, charge transport, catalytic activity, adsorption behaviour, and interfacial reactivity without changing the bulk chemical composition. However, the environmental burden associated with conventional nanoparticle preparation remains a significant limitation. Wet-chemical and high-temperature routes may require toxic reducing or capping agents, generate hazardous residues, or involve energy-intensive processing. Green synthesis has therefore moved beyond being a simple alternative preparation route and is increasingly considered a materials-engineering strategy in which naturally occurring biomolecules participate in nucleation, growth, stabilization, and surface functionalization. Plant extracts are attractive in this context because phenolics, flavonoids, proteins, carbohydrates, alkaloids, organic acids, and other phytochemicals can act collectively as complexing, capping, and structure-directing species [1-5].

Among transition-metal oxides, nickel oxide (NiO) is an important p-type semiconductor with a rock-salt cubic structure and a wide optical band gap commonly reported in the approximate range of 3.6-4.0

eV, depending on preparation conditions, particle dimensions, stoichiometry, and defect concentration [6, 7]. NiO is chemically stable, thermally robust, and electrochemically active, which has enabled its use in photocatalysis, gas sensing, electrochromic devices, batteries, supercapacitors, solar-energy conversion, and optoelectronic systems. At the nanoscale, these functions are strongly structure dependent. Crystallite size and agglomeration determine available surface area, while nickel vacancies, oxygen vacancies, surface hydroxylation, and lattice disorder influence carrier density, recombination pathways, adsorption sites, and photoluminescence response. Recent studies on green-synthesized NiO have similarly shown that changes in plant-derived chemistry and synthesis conditions can produce measurable differences in crystallinity, morphology, optical band gap, defect-related emission, and functional performance [7-11].

The central scientific challenge in plant-mediated NiO synthesis is therefore not merely to demonstrate nanoparticle formation, but to understand how the biological precursor controls the resulting physicochemical properties. Most studies employ a single leaf, seed, flower, or root extract and then relate the final nanoparticle characteristics to the overall phytochemical content of that extract. This approach is useful for establishing feasibility, but it provides limited information on intra-plant variability. Different anatomical parts of the same plant can contain substantially different proportions of cellulose, lignin, proteins, soluble sugars, phenolic compounds, mineral ions, and organic acids. These differences can alter metal-ion complexation, combustion behaviour, local redox chemistry, nucleation density, crystal growth, and particle stabilization. Consequently, nanoparticles produced from different organs of one plant may not be physicochemically equivalent even when precursor concentration, thermal treatment, and synthesis route are held constant. A controlled comparison of plant parts can therefore provide stronger mechanistic evidence than comparisons among unrelated plant species.

Eichhornia crassipes (water hyacinth) is especially relevant for such an investigation. It is a rapidly proliferating aquatic macrophyte widely regarded as an invasive species in tropical and subtropical freshwater systems. At the same time, its biomass contains cellulose, hemicellulose, lignin, proteins, carbohydrates, phenolics, and other oxygen-containing compounds that can participate in metal-ion binding and nanoparticle formation [4, 5, 12]. Converting this problematic biomass into a bioresource for nanomaterial synthesis provides a dual sustainability advantage: it reduces dependence on synthetic processing additives while creating value from an abundant aquatic weed. Recent literature has increasingly explored E. crassipes-derived extracts for green fabrication of inorganic nanomaterials, but the role of its distinct anatomical fractions in controlling NiO formation remains insufficiently resolved [12]. In particular, direct leaf-stem-root comparisons under an identical nickel nitrate-urea combustion environment are scarce.

Green combustion synthesis adds another important dimension to this problem. In nitrate-fuel systems, urea supplies combustible species and promotes a rapid exothermic reaction that can generate oxide products within a short processing time. When a plant extract is introduced into the same reaction mixture, its phytochemicals can influence solution complexation before ignition and may also contribute additional organic fuel, gases, and transient carbonaceous species during combustion. These effects can modify local temperature, nucleation rate, crystallite coalescence, porosity, residual surface groups, and defect generation. Plant-assisted combustion should therefore be evaluated as a coupled chemical process rather than interpreted only as conventional combustion supplemented by a 'green' additive. This distinction is important because defect-sensitive properties of NiO, including optical absorption and photoluminescence, may respond to relatively small changes in oxygen stoichiometry and local coordination.

A further limitation in the existing green-NiO literature is that structural, optical, morphological, and dispersion properties are often discussed independently. For application-oriented interpretation, these characteristics should instead be considered as an interconnected structure-property system. X-ray diffraction provides information on phase purity, lattice parameters, and crystallite size; FTIR identifies residual functional groups and Ni-O bonding; UV-Vis spectroscopy and Tauc analysis probe optical absorption and band-gap behaviour; photoluminescence gives indirect information on radiative recombination and defect-associated states; FESEM and EDX reveal particle morphology, aggregation, and elemental composition; and zeta potential provides an experimentally useful measure of surface charge and colloidal stability. Integrating these measurements enables a more defensible assessment of how the biological synthesis medium affects NiO rather than relying on any single characterization result.

Accordingly, the present study investigates NiO nanoparticles synthesized through a green combustion route using aqueous extracts separately prepared from the leaf, stem, and root of E. crassipes. The experimental design keeps the principal inorganic precursor and combustion fuel system comparable while varying the plant-derived component, allowing the influence of anatomical extract source to be examined systematically. The study compares phase formation, crystallite size, lattice characteristics, functional groups, optical absorption, band-gap energy, defect-related photoluminescence, particle morphology, elemental composition, and zeta potential. The principal objective is to establish whether leaf-, stem-, and root-mediated

synthesis produces distinguishable structure-property signatures and to identify which plant fraction provides the most favourable balance of crystallinity, optical characteristics, morphology, and colloidal stability. This comparative approach strengthens the scientific basis for using E. crassipes not only as a sustainable synthesis reagent but also as a tunable bioresource for engineering NiO nanomaterials for photocatalytic, sensing, optoelectronic, and energy-related applications.

2. Materials and Methods

2.1 Preparation of Nickel Nitrate-Urea Solution

1M of nickel nitrate was prepared with 50 mL of distilled water and 50% urea was mixed with 50 mL of distilled water to prepare the initial solution. Urea has been chosen as fuels to start a combustion reaction along with metal nitrate.

2.2 Preparation of *Eicchornia Crassipes* Plant Extract

The plant Eichhornia crassipes were collected from Annur region which is located in Tamil Nadu, India. The plant collected was thoroughly washed using distilled water multiple times to clean surface contaminants. After the cleaning process the plant was separated in to three parts like leaves, stems and roots. To study the influence bioactive compounds, present in these three plant parts through the synthesis process on nanoparticle's properties the separation was made. Then, each piece was stretched out equally and left in the sun to dry for a certain period of time to make sure all the liquid was gone.

The drying process was continuously monitored to prevent microbial growth and degradation of the bioactive components. Once thoroughly dried, the leaves, roots, and stems were individually ground into a fine powder using a mechanical grinder. Separate extracts were prepared for each part by stirring a specific amount of powdered material in distilled water for 30 minutes. The extracts were filtered to remove solid residues and stored for further use. The composition used for each part was Root extract 7.2747 g, Stem extract 7.5460 g and Leaf extract: 7.27701 g. Each extract was prepared in 50 mL of distilled water.

2.3 Combustion Process

The combustion process is a high-temperature exothermic redox chemical reaction between a fuel and an oxidant, usually in an atmospheric oxygen. The plant extracts are shown in Figure 1.

The prepared Eichhornia crassipes extract (root, stem, and leaf) was separately added to parallel nickel nitrate-urea solutions under constant stirring on a sonicator for 30 minutes. The obtained homogenous solutions of each part of the extract were separately transferred to a furnace and subjected to a combustion reaction at approximately 400–600°C. The combustion process resulted in the formation of nickel oxide (NiO) nanoparticles. The reaction proceeded with the evolution of gases, leaving behind a fine powder.

Mechanism of the Reaction

$$Ni(NO_3)_2{\cdot}6H_2O \rightarrow NiO + 2NO_2 + \tfrac{1}{2}O_2 + 6H_2O$$

$$CH_4N_2O + O_2 \rightarrow CO_2 + 2NH_3$$

$$2NH_3 + 3/2O_2 \rightarrow N_2 + 3H_2O$$

$$C_xH_yO_z + O_2 \rightarrow CO_2 + H_2O$$

Combustion Process

$$Ni(NO_3)_2{\cdot}6H_2O + CH_4N_2O + \text{PLANT EXTRACT} + O_2 \rightarrow NiO + NO_2 + CO_2 + N_2$$

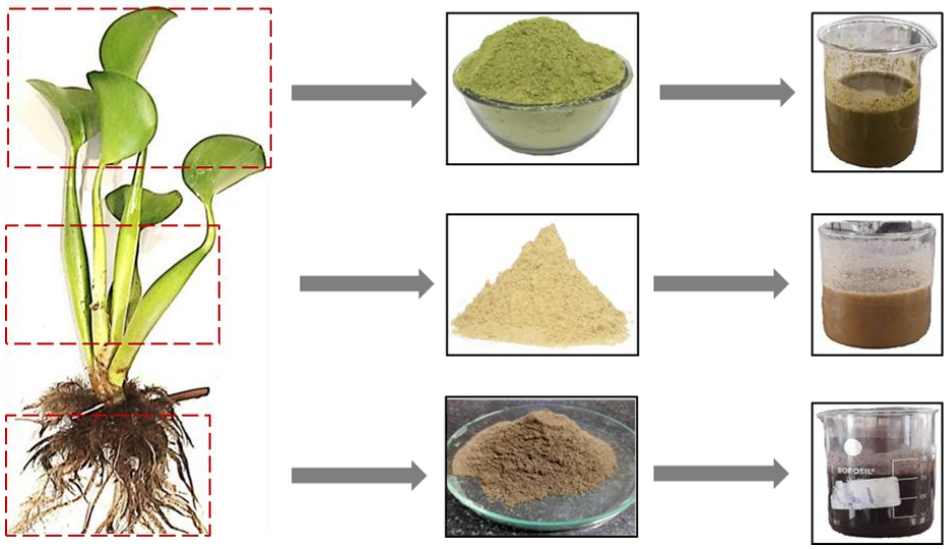

Figure 1. Plant Extraction Method

2.4 Characterization Techniques

The prepared nanoparticles were subjected to various characterization techniques to study their structural, optical, thermal, vibrational and morphological properties through XRD, UV-vis, FTIR, PL, TG-DTA, FESEM and Zeta potential.

3. Result and Discussion

3.1 X Ray Diffraction Analysis

The X-ray diffraction (XRD) of the synthesised NiO nanoparticles shown in Figure 2 derived from the plant portions of Eichhornia crassipes (EC) showed that the structures of NiO was successfully synthesised.

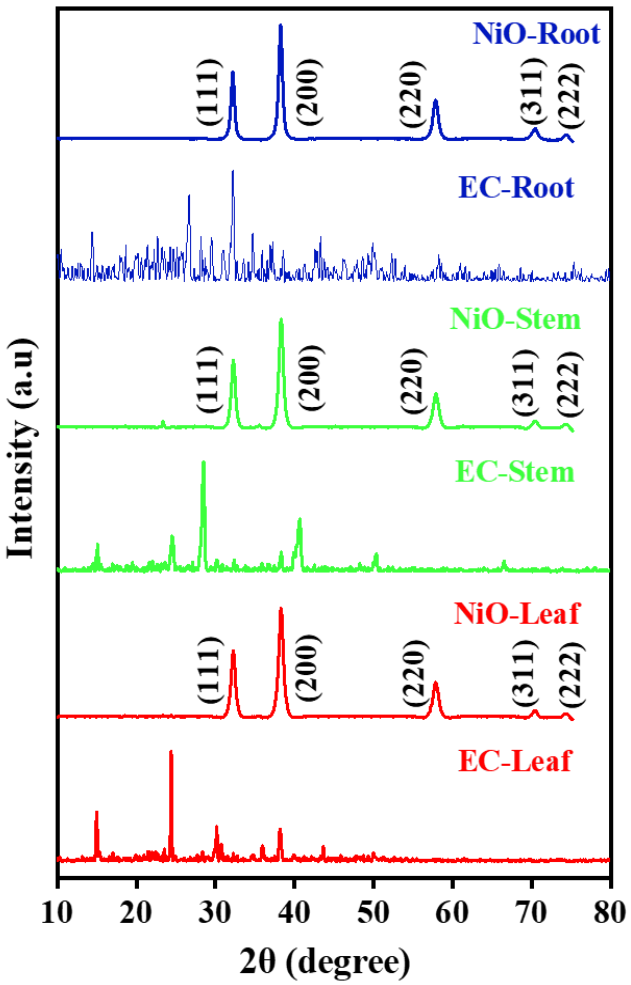

Figure 2. Shows the x ray diffraction analysis of synthesized NiO nanoparticles and the plant parts of Eichhornia crassipes (EC).

The XRD patterns obtained from the plant extracts, namely EC-Root, EC-Stem and EC-Leaf, exhibited multiple broad and low-intensity peaks, indicating the presence of an amorphous or semi-crystalline structure. The obtained peaks may be ascribed to the existence of organic and bioactive compounds in all three parts of the plant. The other minor peaks indicate the presence of different phytochemicals or residual mineral elements in the plant extracts [7, 8].

The XRD pattern of the green synthesized nickel oxide nanoparticles through different plant part extracts like Root assisted NiO, Stem assisted NiO and Leaf assisted NiO confirm the single-phase cubic structure with higher crystallinity. The presented spectra confirmed the NiO phase with reported data [13]. The formation of NiO phase has been verified by the Rietveld refinement of XRD patterns. The refined XRD profiles are shown in Figure 3 (a-c), while the corresponding refined crystal structures are illustrated in Figure 4 (a-c). The experimental XRD patterns exhibit a series of well-defined diffraction reflections characteristic of crystalline NiO. The major reflections can be indexed to the (111), (200), (220), (311), and (222) crystallographic planes of cubic NiO appeared at 32.5°, 38.2°, 57.6°, 70.1°, and 74.3°. These reflections are consistent with the characteristic rock-salt structure of NiO, in which Ni and O ions occupy the cationic and anionic sites of a face-centred cubic framework. The absence of additional intense reflections attributable to other crystalline phases indicates that the synthesized products predominantly possess the NiO phase. The refinement parameters along with the lattice parameters are summarized in Table 1. The close agreement between the observed and calculated profiles and the small difference curves confirm the suitability of the adopted structural model. In Figure 4, white solids represent Ni atoms and red solids represent O atoms.

The average crystallite size (D) of the NiO nanoparticles was determined using the Scherrer equation.

$$D = D = \frac{R\lambda}{\beta cos\ \theta} \quad (1)$$

Where K is the shape factor (typically 0.9), λ is the X-ray wavelength (1.5406 Å for Cu Kα radiation), β is the full width at half maximum (FWHM) of the diffraction peak in radians, and θ is the Bragg angle.

The process of making nickel oxide (NiO) nanoparticles from extracts of different parts of the Eichhornia crassipes plant resulted in average crystallite sizes of about 13.6 nm for NiO-Leaf, 17.3 nm for NiO-Stem, and 14.1 nm for NiO-Root. These differences in crystallite size suggest that the phytochemical makeup of each plant part affects how nanoparticles form and grow. We used Bragg's equation to figure out the interplanar spacing (d-spacing):

$$n\lambda = 2d\ sin\ \theta \quad (2)$$

Where n is the order of diffraction (usually 1), λ is the X-ray wavelength, θ is the Bragg angle, and d is the distance between the planes. The d-spacing values for the main diffraction peaks confirmed that the NiO phase was present. The Joint Committee on Powder Diffraction Standards (JCPDS) Card No. 47-1049 [14] says that the d-spacing values for NiO are 2.41 Å for the (111) plane, 2.09 Å for the (200) plane and 1.48 Å for the (220) plane.

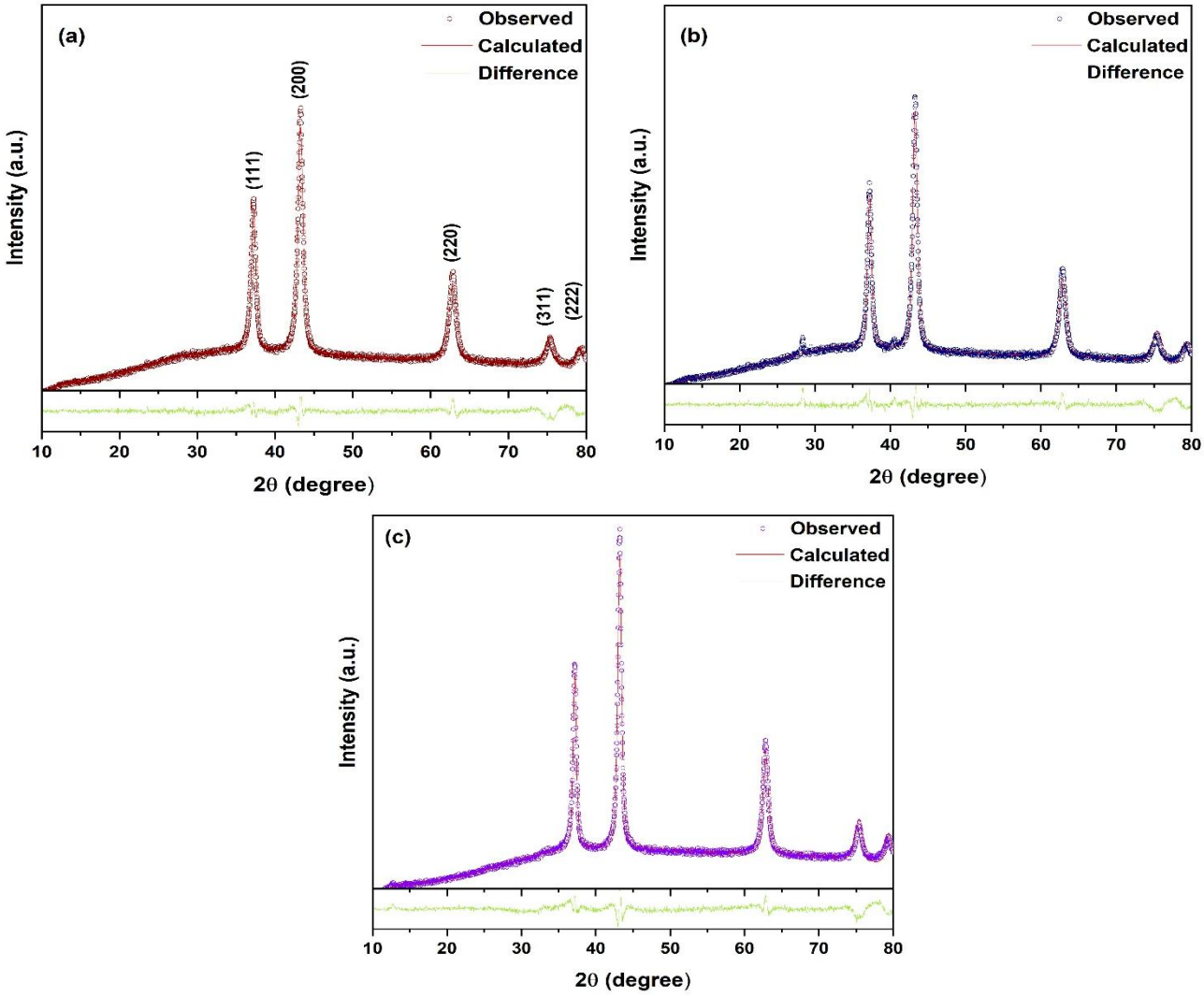

Figure 3. Refined XRD pattern of NiO nanoparticles synthesised using **(a)** Leaf, **(b)** Stem and **(c)** Roots of Eichhornia crassipes plant.

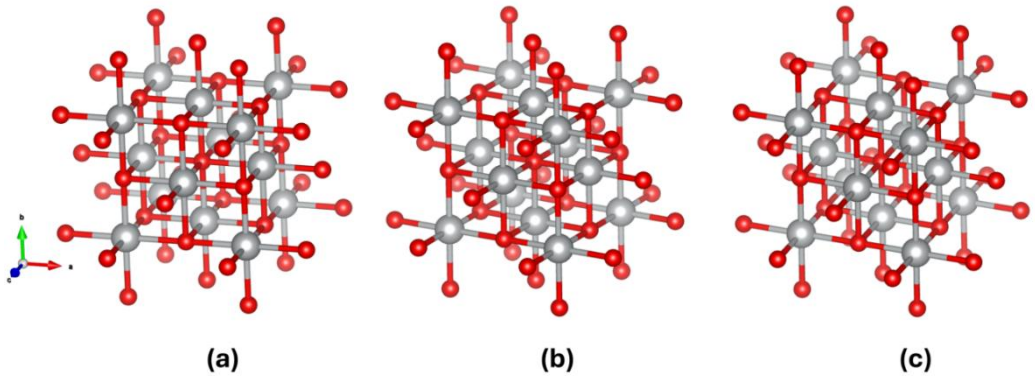

Figure 4. Refined structures of NiO nanoparticles synthesised using **(a)** Leaf, **(b)** Stem and **(c)** Roots of Eichhornia crassipes plant.

Table 1. Refinement parameters and lattice parameter of NiO nanoparticles.

Sample	R_{exp}	GoF	R_{wp}	χ^2	*a* (Å)
L-NiO	3.02	1.98	2.33	1.53	4.18098
S-NiO	3.32	2.03	2.67	1.64	4.18012
R-NiO	3.58	1.98	2.27	1.71	4.17724

The d-spacing value of 2.41 Å for the (111) plane indicates the existence of this primary NiO reflection.

The lattice parameter a for the cubic NiO structure was determined using the equation:

$$a = d\sqrt{h^2 + k^2 + l^2} \quad (3)$$

The Miller indices confirm the lattice parameters values of all three NiO nanoparticles synthesized through different plants extract are well matched with the standard cubic NiO lattice constant (about 4.57 Å, JCPDS 47-1049). This shows that a pure NiO phase was formed without any major distortions. The small differences in lattice constants (see Table 1) suggest that the crystal structure has very little strain or defects, which means the synthesized NiO nanoparticles are highly crystalline in nature. The fluctuations in the bond lengths can be clearly observed in Figure.4 which can affect the unit cell resulting to changes in the lattice parameter. Generally, Eichhornia crassipes (water hyacinth) have major chemical compositions of carbon, lignin, protein and cellulose. These chemical compositions particularly cellulose may be the active source for the formation of crystalline nature of present NiO nanaoparticles and changes in the crystallite sizes.

3.2 FT-IR Analysis

Fourier Transform Infrared Spectroscopy (FTIR) was employed to identify the functional groups present in the Eichhornia crassipes extract and to confirm the successful formation of nickel oxide (NiO) nanoparticles. This technique helps in understanding the chemical composition of the plant extract before combustion and assessing the removal of organic compounds after the synthesis process. Figure 5 shows the FTIR spectra of EC-Root, EC-Stem, and EC-Leaf, along with their respective NiO derivatives, were analysed to determine the differences in functional groups before and after combustion. Functional Groups from Plant Compounds (EC-Root, EC-Stem, EC-Leaf). These peaks come from organic compounds present in Eichhornia crassipes extract O–H stretching (~3200–3600 cm^{-1}) → Hydroxyl (-OH) from water, alcohols, or phenolic compounds [7]. The C=O stretching (~1600–1700 cm^{-1}) → Carbonyl (C=O) from flavonoids, ketones, or carboxylic acids [15]. The C–H bending (~1400 cm^{-1}) → Alkane (-CH2 or -CH3) groups from plant-derived hydrocarbons [9]. The C–N or N–H (~1100–1300 cm^{-1}) → Amine (-NH) or C–N stretching from proteins or nitrogen-containing compounds in the plant [16].

Functional Groups from NiO Nanoparticles (EC-Root-NiO, EC-Stem-NiO, EC-Leaf-NiO) After combustion, the organic compounds are mostly removed, leaving NiO features Ni–O stretching (~500–600 cm^{-1}) → Confirms the formation of NiO nanoparticles [17].

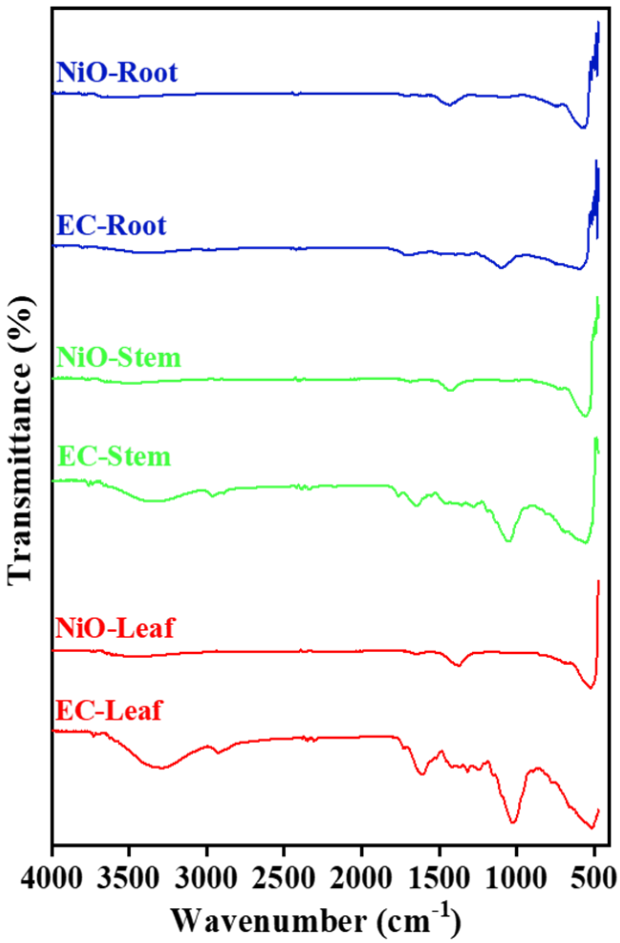

Figure 5. Shows the FTIR analysis of synthesized NiO nanoparticles and the plant parts of Eichhornia crassipes (EC).

The O–H stretching band (~3200–3600 cm^{-1}) → Surface hydroxyl groups from adsorbed moisture. Weak residual organic peaks (~1400–1700 cm^{-1}) → Traces of organic material that were not fully removed. The FTIR analysis successfully verified the conversion from plant-derived precursors to nickel oxide nanoparticles. The absence of significant organic functional group peaks and the emergence of a distinct Ni–O stretching band in the synthesized NiO samples signify the effective elimination of organic compounds and the generation of NiO nanoparticles. If there are still organic peaks, it means that more purification steps, like more calcination or washing, are needed to get very pure NiO. This FTIR characterization helps confirm the structure and chemistry of the material that was made.

3.3 Uv Spectroscopy and Bandgap Analysis

We used UV-visible (UV-Vis) spectroscopy to look at the optical properties of the nickel oxide (NiO) nanoparticles we made. Figure 6 displays the absorption spectra of the three distinct NiO samples: NiO-Leaf, NiO-STEM, and NiO-Root, each exhibiting unique absorption peaks, thereby validating the successful synthesis of nanoscale NiO. For each sample, the recorded absorption maxima (λmax) were 311 nm for NiO-Leaf,

312 nm for NiO-STEM, and 315 nm for NiO-Root. The change in absorption peaks indicates that the size, shape, and crystallinity of the nanoparticles are different. The NiO-Root sample had the highest redshifted absorption peak at 315 nm. This could mean that the average particle size is bigger or that there are more defect states, which would make the energy transition slightly lower. NiO-Leaf and NiO-STEM, on the other hand, had absorption peaks that were slightly blue-shifted. This could be due to smaller particle sizes and quantum confinement effects.

The energy bandgap (E_g) was determined using Tauc's relation:

$$(\alpha h\nu)\, n \;=\; A(h\nu - Eg) \qquad (4)$$

where 'α' is the absorption coefficient, hv is Planck's constant, 'v\v' is the photon frequency, 'A' is a constant, and 'n' is the exponent depending on the nature of electronic transitions. For NiO, which exhibits a direct bandgap, n=2n was used. The Tauc plot of synthesized NiO nanoparticles is shown in figure 7.

The calculated bandgap values for each sample were 3.37 eV for NiO-Leaf (Moderate bandgap), which means that the crystallinity and particle size distribution were balanced. 3.40 eV for NiO-STEM (highest bandgap), which means the particles are smaller and the crystals are better. 3.38 eV for NiO-Root (Slightly lower bandgap) with a redshifted absorption peak (315 nm), which could be because of defect states or bigger particle aggregation. These bandgap values are a little higher than the bulk NiO bandgap (~3.1–3.3 eV) that has been reported, which shows how quantum confinement works in nanostructures [18]. NiO-STEM had the highest bandgap value (3.40 eV), which means that the nanoparticles were probably smaller and more crystalline [19, 20]. The NiO-Root sample, which had the most redshifted absorption, had a bandgap of 3.38 eV, which was a little lower than the others. This could be because there were more surface defects or particles stuck together [21]. NiO nanoparticles made from plant extracts have been shown to have bandgap values between 3.30 and 3.50 eV, depending on the size of the particles and the conditions under which they were made. NiO nanoparticles that are made in a lab usually have bandgap values between 3.2 and 3.4 eV, which depends on the temperature of calcination and the concentration of the precursor [19, 20]. The small difference in bandgap between NiO-Leaf, NiO-STEM, and NiO-Root suggests that they have different levels of crystallinity, oxygen vacancies, and defect states, which can affect how they look. The UV-Vis absorption spectra and bandgap analysis showed that NiO nanoparticles with different optical properties had been made successfully.

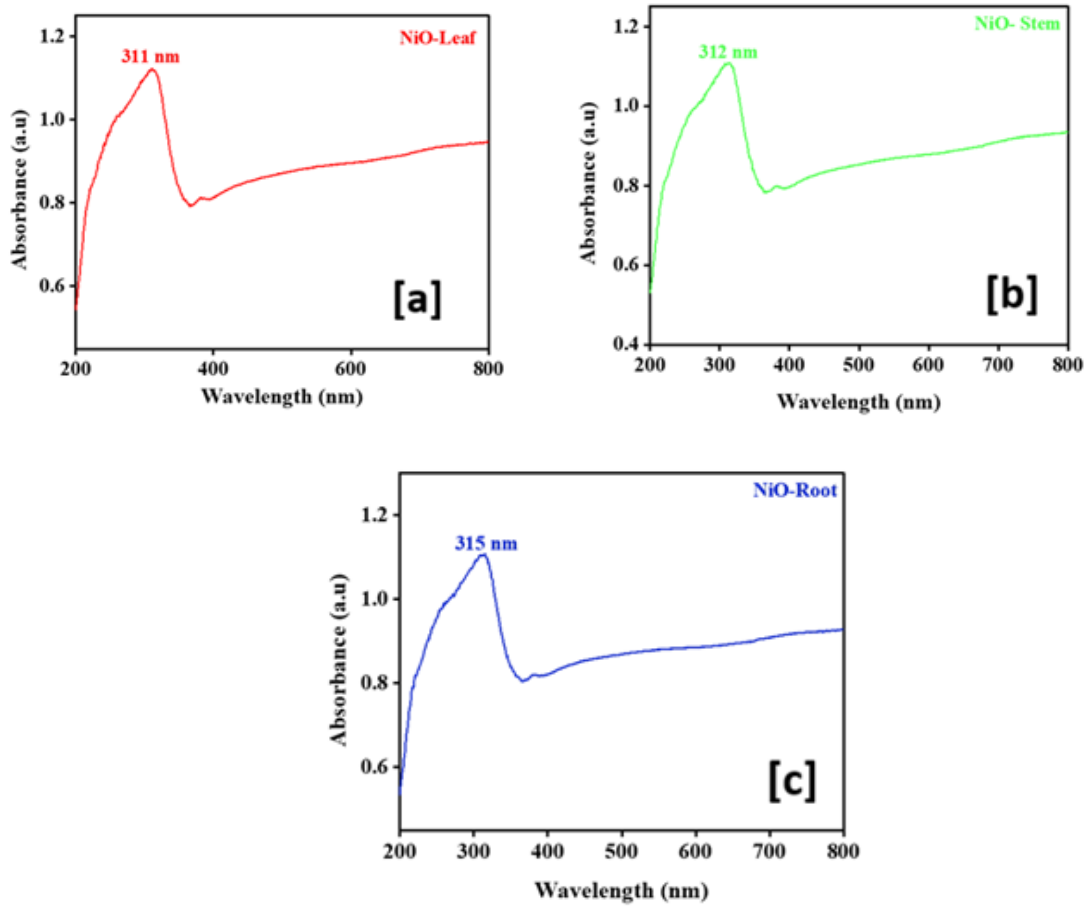

Figure 6. Shows the UV Vis absorption spectra of synthesized NiO nanoparticles.

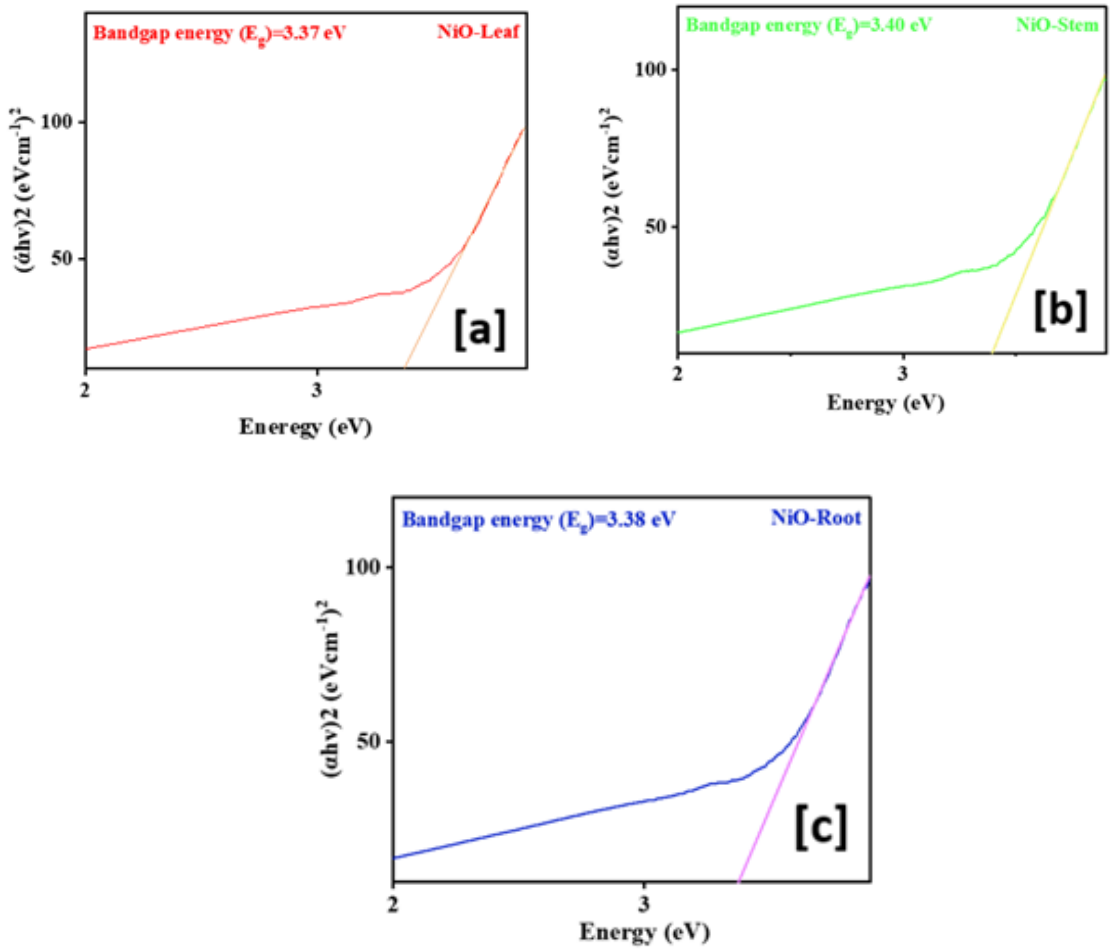

Figure 7. Shows the Tauc plot of synthesized NiO nanoparticles.

3.4 Photoluminescence Analysis

The photoluminescence (PL) spectra of NiO nanoparticles synthesized (Figure 8) from leaf, stem, and root extracts display pronounced UV and violet emission peaks, thereby validating the creation of defect-rich NiO nanostructures. There are big differences in the positions and intensities of emissions depending on the precursor plant extract. This shows that it has an effect on how defects form and how light behaves. Figure 8(b) shows that the NiO-Leaf sample has three strong emission peaks at 311 nm, 361 nm, and 391 nm. The emission at 311 nm is due to intrinsic band-to-band transitions in NiO [22]. The 361 nm near-UV emission is linked to nickel vacancies and self-trapped excitons [19, 22], while the violet emission at 391 nm is linked to oxygen vacancies and lattice distortions in the NiO structure [10]. The blue emission at 443 nm that was seen in the EC-Leaf extract (Figure 8(a)) is no longer there, which shows that all of the organic fluorophores broke down completely during the combustion synthesis process [7]. The violet emission (391 nm) that is slightly blue-shifted compared to NiO-Stem (393 nm) and NiO-Root (395 nm) suggests that there are fewer oxygen vacancies in the leaf-derived NiO sample [11]. Figure 8(d) shows that the NiO-Stem sample has four clear emission peaks at 314 nm, 354 nm, 375 nm, and 393 nm. This means that the structure has changed more [19]. The 314 nm peak comes from intrinsic band-to-band transitions, and the 354 nm emission comes from nickel vacancies and self-trapped excitons [10]. Oxygen interstitials and surface defect states are what cause the 375 nm UV emission. The violet emission at 393 nm is often linked to oxygen vacancies and distortions in the lattice [23]. The lack of the 434 nm blue emission (which is in EC-Stem Figure 8(c)) shows that organic parts were removed when the nanoparticles were made [24]. The relatively strong 393 nm emission shows that there are more oxygen vacancies than in NiO-Leaf, which means that the defect density is higher in stem-derived NiO nanoparticles [25]. The NiO-Root sample has three main emission peaks at 324 nm, 369 nm, and 395 nm, as shown in Figure. 8(f). The 324 nm emission is due to intrinsic electronic transitions between bands [22]. The 369 nm near-UV emission comes from nickel vacancies and states caused by defects [7]. The strong violet emission at 395 nm is due to oxygen vacancies and lattice distortions [11]. The loss of the 439 nm blue emission seen in EC-Root (Figure 8(e)) is more proof that organic compounds break down during synthesis [25].

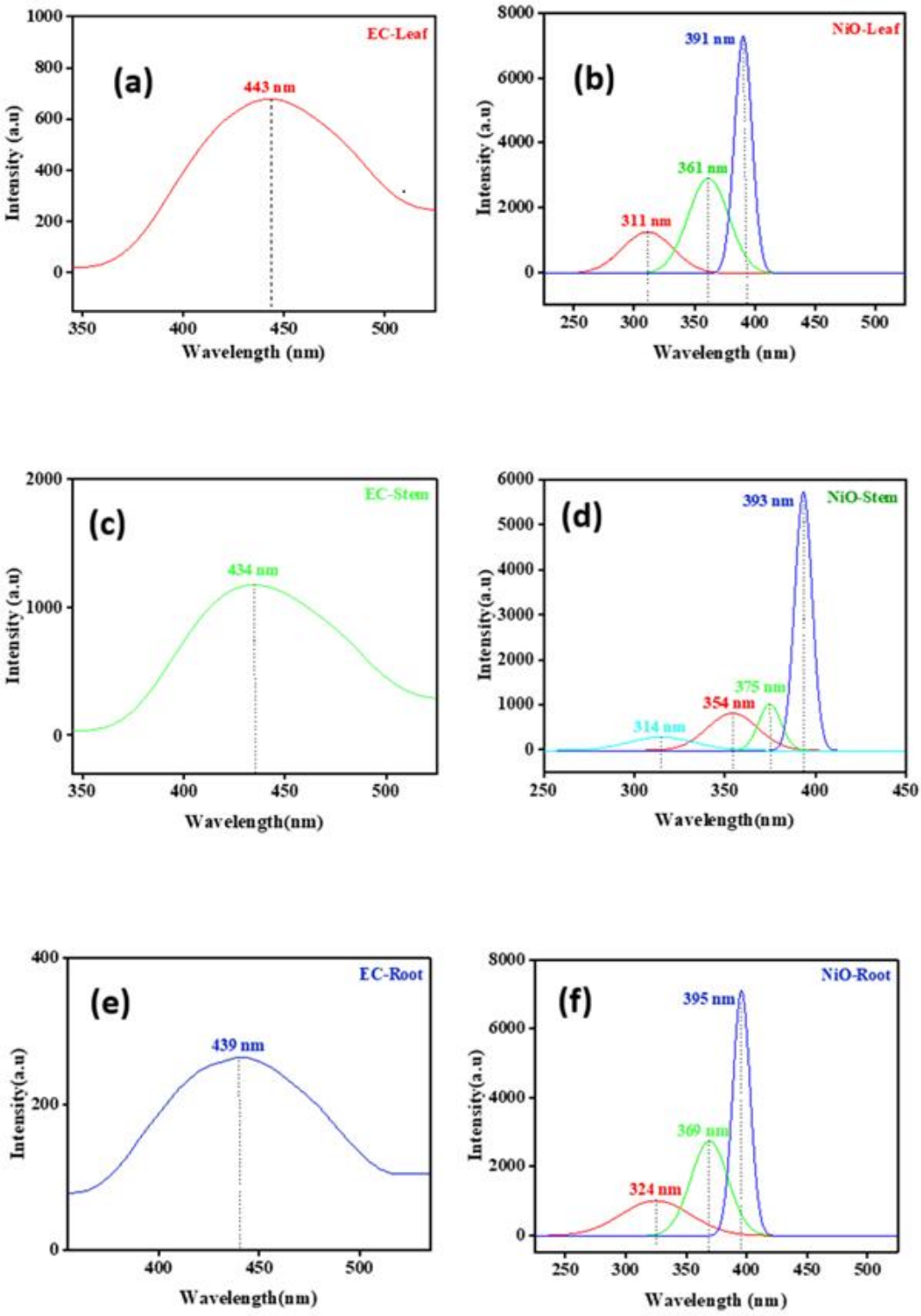

Figure 8. Photoluminescence analysis of synthesized NiO nanoparticles and the plant parts of Eichhornia crassipes (EC)

The 395 nm peak is a little bit red-shifted compared to the NiO-Stem (393 nm) and NiO-Leaf (391 nm) peaks. This means that the root-derived NiO nanoparticles have a higher concentration of oxygen vacancies [13]. A comparative analysis shows that the violet emission peaks for the samples NiO-Leaf, NiO-Stem, and NiO-Root are moving in a systematic way: 391 nm, 393 nm, and 395 nm, respectively. This gradual redshift shows that the concentration of oxygen vacancies is higher in NiO nanoparticles that come from the leaf than in those that come from the root [10]. The differences in emission characteristics show how important the composition of plant extracts is in

controlling defect formation during green combustion synthesis.

The disappearance of blue emissions (434–443 nm) in all NiO samples confirms the complete decomposition of organic fluorophores present in the crude extracts, ensuring the formation of phase-pure NiO nanoparticles [24]. Overall, the strong UV and violet emissions observed in all three samples confirm the formation of defect-engineered NiO nanoparticles [26]. Among them, NiO-Root exhibits the highest defect density, followed by NiO-Stem and NiO-Leaf. These defect-induced optical properties make the synthesized NiO nanoparticles promising candidates for applications in UV photodetectors, optoelectronic devices, sensors, and photocatalytic systems.

3.5 Field Emission Scanning Electron Microscopy (Fe-Sem)

The morphological structure and particle size of the nanoparticles were both analysed using the FE-SEM. According to the FESEM observations, NiO nanoparticles made with plant parts of Eichhornia crassipes from leaves, stems, and roots primarily have a spherical shape, however there are discernible variations in the samples aggregation patterns and structural configurations [27]. The leaf derived NiO nanoparticles exhibit mild aggregation and well-defined spherical particles shown in Figure 9 [28].

The stem derived NiO nanoparticles show a relatively uniform particle distribution with spherical morphology shown in Figure 10 [29]. The observed porosity in FESEM images suggests the potential for high surface area applications [30]. The root extract derived NiO nanoparticles shown in Figure 11 exhibit a denser network of nanoparticles with visible clustering and spherical morphology. The morphology suggests a strong interaction between nanoparticles, possibly due to biomolecules from the root extract [29].

The Eichhornia crassipes Leaf, stem and root derived NiO nanoparticles show better control over particle size (~13 nm), while root-derived NiO produces larger particles (~24 nm) respectively shown in Figure 12 [27]. Stem-derived NiO detected the smallest and most uniform particles [30]. Root-based NiO exhibits high polydispersity, suggesting synthesis conditions led to larger particle growth or aggregation. Smaller NiO particles (leaf & Stem) are better suited for high-surface-area applications [31]. The elemental composition detected in EDX (Figure 13) suggests the presence of Ni, O and organic residues from the plant, which may influence the final nanoparticle structure. The porous and rough surface may enhance their catalytic and adsorption properties [12].

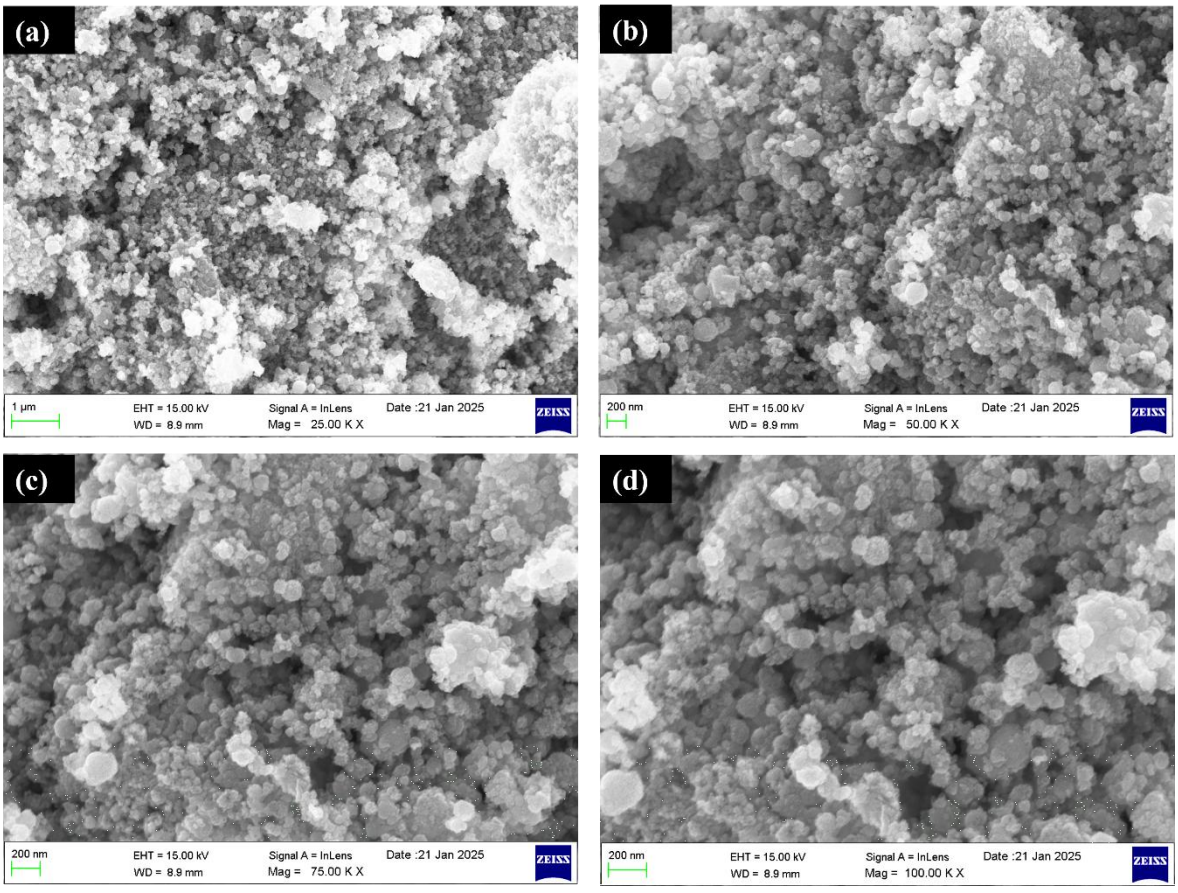

Figure 9. FESEM analysis at different magnifications of Eichhornia crassipes Leaf derived NiO nanoparticles

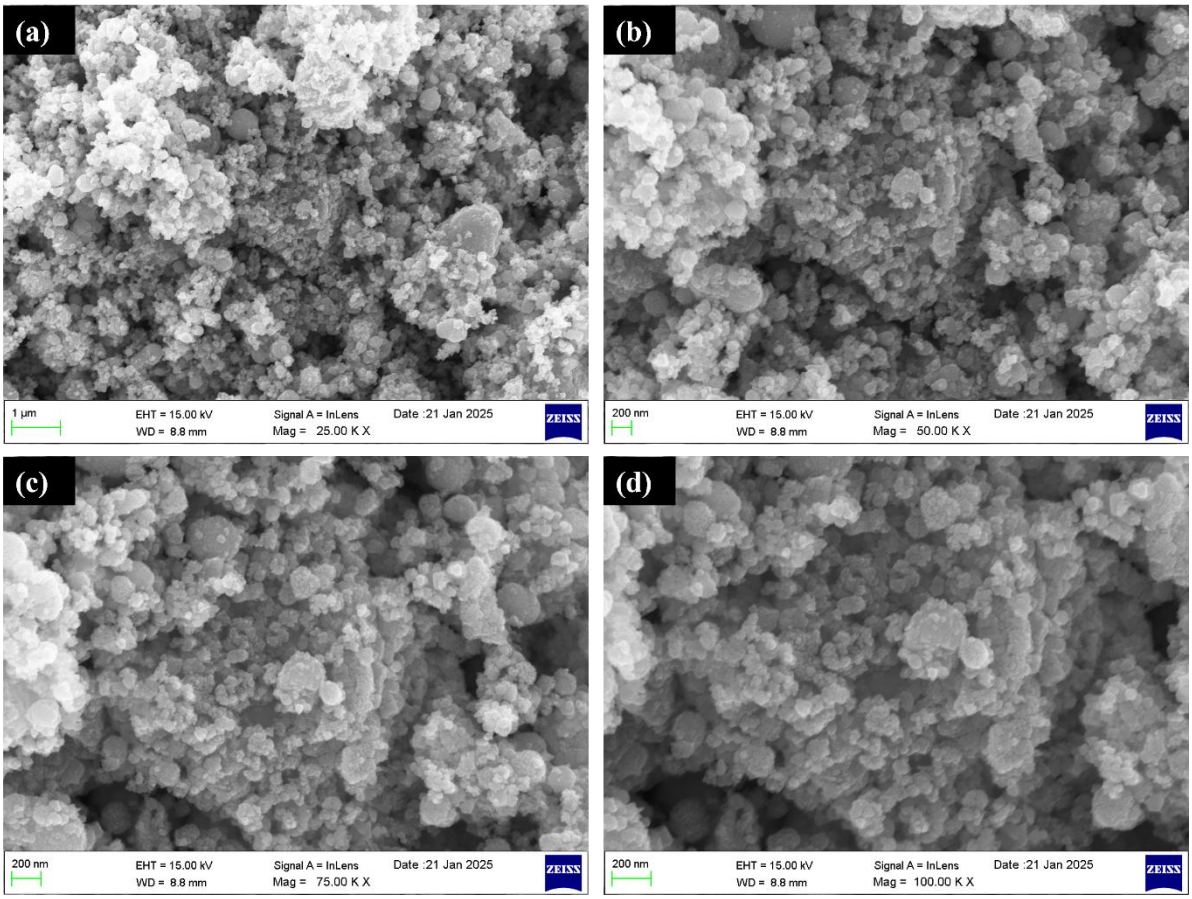

Figure 10. Shows the FESEM analysis at different magnifications of Eichhornia crassipes Stem derived NiO nanoparticles.

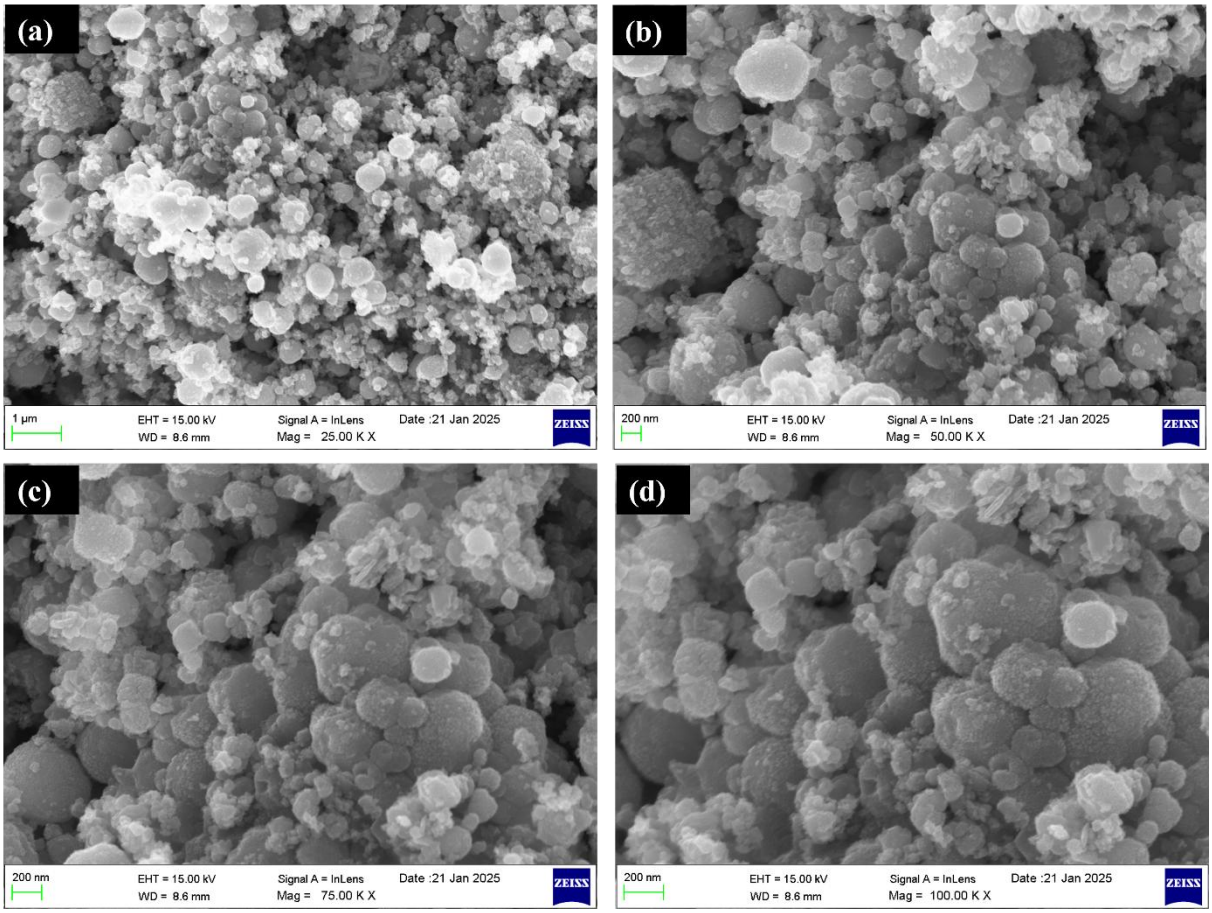

Figure 11. FESEM analysis at different magnifications of Eichhornia crassipes Root derived NiO nanoparticles.

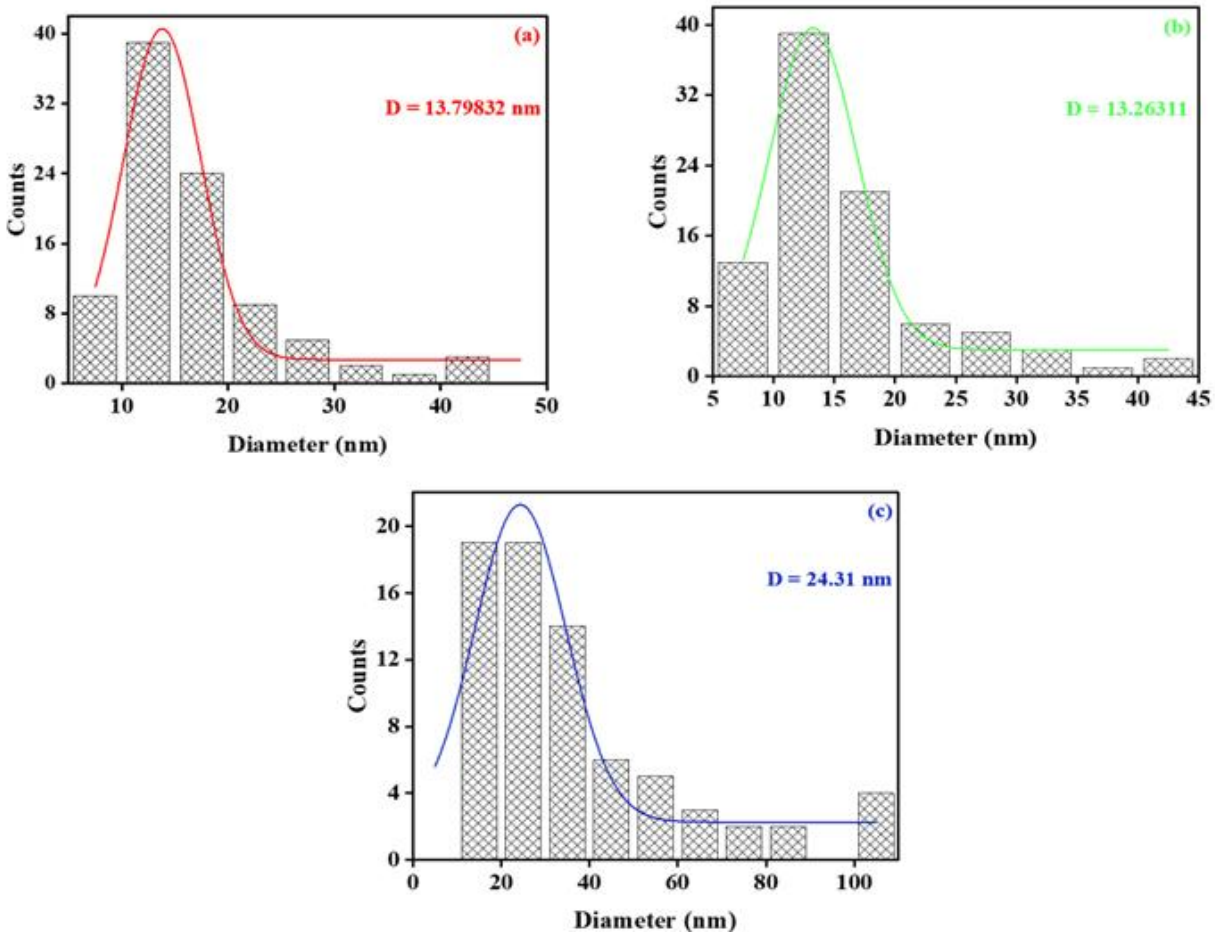

Figure 12. FESEM analysis of Eichhornia crassipes leaf, stem and root derived NiO nanoparticles particle size distribution through a histogram.

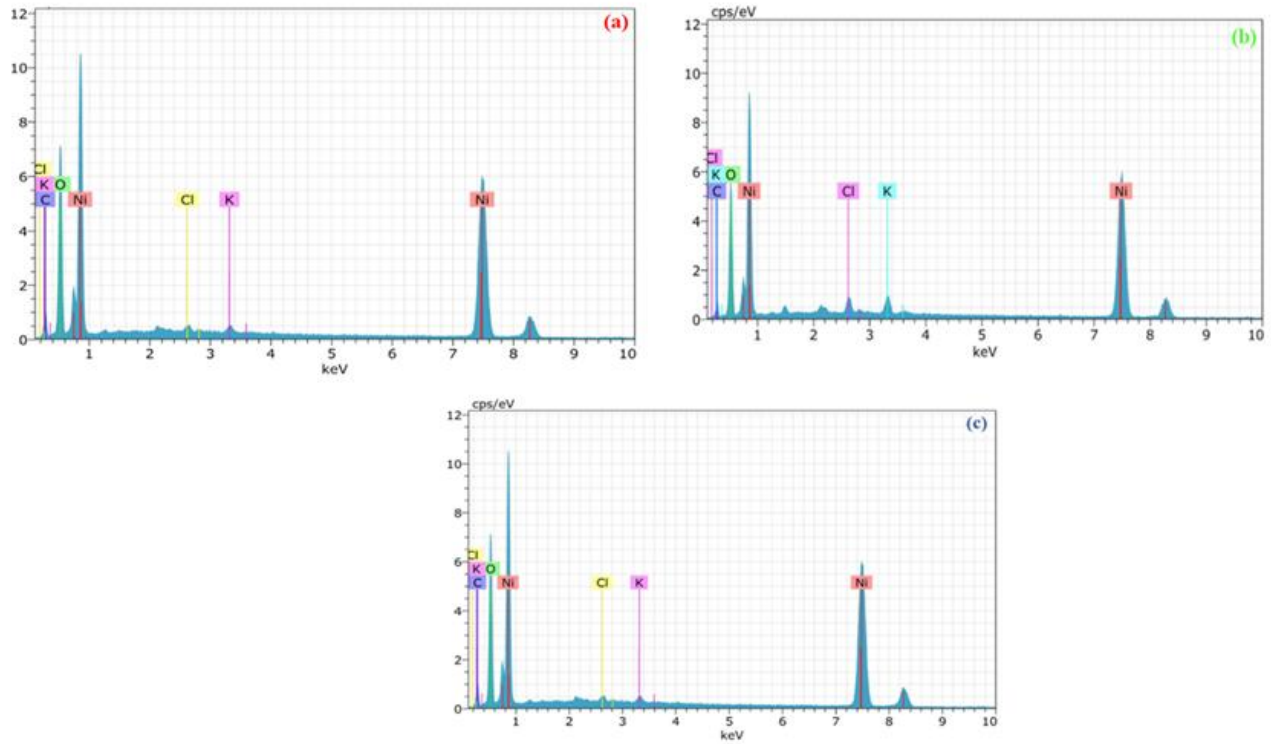

Figure 13. EDX analysis of Eichhornia crassipes **(a)** leaf, **(b)** stem and **(c)** root derived NiO nanoparticles

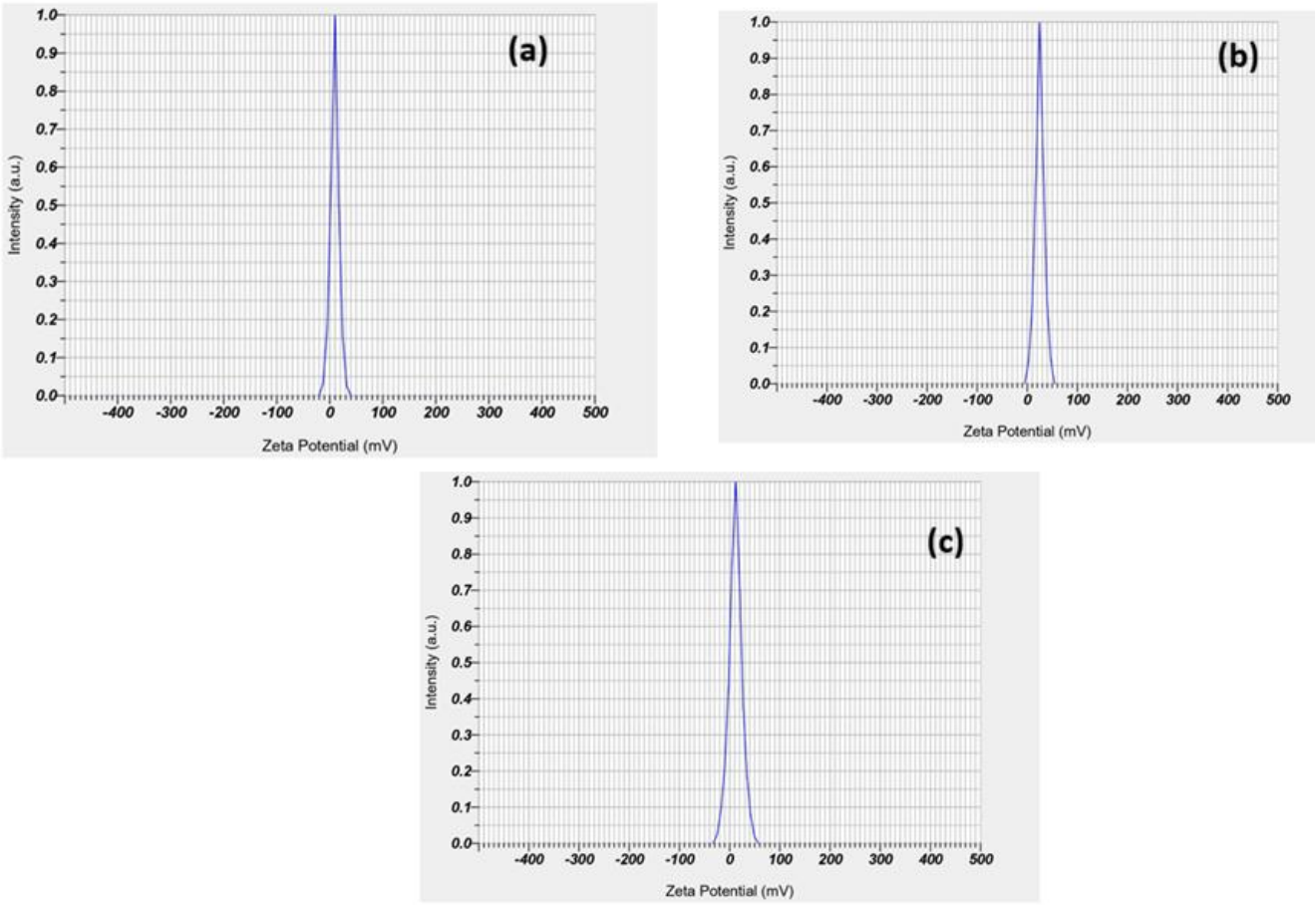

Figure 14. Zeta potential of Eichhornia crassipes **(a)** leaf, **(b)** stem and **(c)** root derived NiO nanoparticles.

3.6 Zeta Potential

Figure 14 (a-c) shows the colloidal stability analysis of NiO nanoparticles prepared through three different plant parts. The Zeta potential values are different for all three samples. Figure 14(a) displays the Zeta potential of NiO nanoparticles derived from EC-Leaf. It has been recorded as +9.5 mV which means the particles are not very stable in suspension and don't repel each other very well. This could cause particles to clump together, which would modify how reactive they are and how much surface area they have in sensors and catalysts. In general, a zeta potential of more than 30 mV (either positive or negative) signifies that the object is very stable and repels other objects quite strongly. Values that are near to zero, on the other hand, suggest that particles are coming together [32].

The colloidal stability values of NiO nanoparticles using three different plant parts extract such as 9.5 mV (leaf), 11.7 mV (root) and 24.9 mV (stem), which shows that the colloidal stability of stem assisted NiO nanoparticles has higher stability than the other two NiO nanoparticles. The Zeta potential studies confirms that all the NiO nanoparticles synthesized through leaf extract, stem extract and root extract are p-type semiconductor nature. Among these three samples, NiO nanoparticles assisted through stem transfer more charges due to higher zeta potential and electrophoretic mobility [33, 34].

4. Conclusion

Green synthesized NiO nanoparticles through *Eichhornia crassipes plant* parts (leaf, stem and root) extract has been reported. The structural, optical, colloidal stability, thermal and morphological analysis of NiO nanoparticles were analyzed. The effect of different plant part extracts on their physicochemical properties has been studied. The XRD analysis confirmed that the NiO nanoparticles have a single-phase cubic structure with higher crystalline nature. The average crystallite sizes of NiO nanoparticles prepared through different extracts are range between 13 and 17 nm. The FTIR spectra of NiO and different plant parts confirms the functional groups present. It confirms the Ni-O stretching vibrations for all three sample in the between 400 to 600 cm-1. The optical properties of NiO nanoparticles assisted through three plant extracts have been analyzed through UV-Vis and PL spectroscopies. The optical band gap values of NiO nanoparticles using various extract were found in the range between 3.40 to 3.37 eV. The external morphology of the samples was recorded through FESEM, which showed that most of the nanoparticles were mostly spherical, they grouped together in varied ways depending on the plant extract

employed. The higher colloidal stability about 24.9 mV was obtained by stem assisted NiO nanoparticles and all the three samples show the p-type semiconductor nature of NiO nanoparticles. The obtained results confirms that extracts from *Eichhornia crassipes* can be utilized to synthesis NiO nanoparticles with good physicochemical properties for photocatalysis, sensors, optoelectronics, and energy devices.

References

[1] M. Boudiaf, Y. Messai, E. Bentouhami, M. Schmutz, C. Blanck, L. Ruhlmann, H. Bezzi, L. Tairi, D.E. Mekki, Green synthesis of NiO nanoparticles using Nigella sativa extract and their enhanced electro-catalytic activity for the 4-nitrophenol degradation. Journal of Physics and Chemistry of Solids, 153, (2021) 110020. https://doi.org/10.1016/j.jpcs.2021.110020

[2] G. Gürsoy, Z. Çiçek, S. Tekerek, E. Kiray, A. Tanriverdi, E. Çakmak, Synthesis of NiO nanoparticles from Paulownia tomentosa plant extracts via a green synthesis method and antibacterial, antibiofilm and cytotoxicity applications. Applied Organometallic Chemistry, 38(6), (2024) e7492. https://doi.org/10.1002/aoc.7492

[3] M. Bhoye, S. Pansambal, P. Basnet, K-YA Lin, KY Gutierrez-Mercado, A Pérez-Larios, A Chauhan, R Oza, S Ghotekar. Eco-Friendly Synthesis of Ni/NiO Nanoparticles Using Gymnema sylvestre Leaves Extract for Antifungal Activity. Journal of Composites Science, 7(3), (2023) 105. https://doi.org/10.3390/jcs7030105

[4] S. Mohan, K. Indira, D. Rajeswari, S. Sivakumar, A. Manickam, Sustainable synthesis of nickel oxide nanoparticles using Abrus precatorius seed extract: Antioxidant and antibacterial potential. Results in Materials, 28, (2025) 100805. https://doi.org/10.1016/j.rinma.2025.100805

[5] A.B. Habtemariam, M. Oumer, Plant Extract Mediated Synthesis of Nickel Oxide Nanoparticles. Materials Intrnational, 2(2), (2020) 0205-0209.

[6] A. Khalaf, R. Saghir, A.M. Abdallah, M. Noun, R. Awad, Influence of Mo doping on the structural, Raman scattering, and magnetic properties of NiO nanostructures, Applied Physics A, 130, 691 (2024). https://doi.org/10.1007/s00339-024-07816-w

[7] T.E. Gebremichael, E. Tesfaye, T. Abebe, A. Bekele, Z.H. Robi, T.E. Gebremikael, Bio-derived NiO nanoparticles from Colocasia esculenta leaf extract with enhanced antibacterial activity and efficient photocatalytic degradation of methylene blue. RSC advances, 16(3), (2026) 2030-2043. https://doi.org/10.1039/d5ra08840b

[8] S. Agalya, L.C. Nehru, S. Sagadevan, Green-synthesized nickel oxide nanoparticles for sustainable wastewater treatment and enhanced bacterial control. Ceramics International, 50(23), (2024) 50185-50199. https://doi.org/10.1016/j.ceramint.2024.09.365

[9] A. Berhe, F. Tilahun, A. Wendu, W. Lakew, Plant-mediated biosynthesis of Nickel (II) oxide nanoparticles from Calpurnia Aurea Leaf extract: A promising photocatalyst for malachite green degradation. Chemical Physics Impact, 11, (2025) 100906. https://doi.org/10.1016/j.chphi.2025.100906

[10] I. Kapil, P. Yadav, S. Vats, G. Sharma, A. Das, S. Bera, M. Dutta, A. Bhaduri, Green approaches to nickel oxide nanoparticles: Visible-light-driven photocatalytic degradation of brilliant green, methyl orange dyes and antibiotic ciprofloxacin, Catalysis Today, 468 (2026) 115696. https://doi.org/10.1016/j.cattod.2026.115696

[11] V.K. Mohan, T. Srinivas, A. Gupta, V. Khedekar, J. Llorca, T.T. John, Defect tailored NiO quantum Dots via Energy-Efficient synthesis: electronic transport and selective cytotoxicity. ACS omega, 10(32), (2025) 36697. https://doi.org/10.1021/acsomega.5c05954

[12] A.S. Nair, A. Syama, R.R. Prabhu, A Comprehensive Review on Green Synthesis of Nanoparticles from Eichhornia crassipes as a Potential Management Strategy to Negate the Adverse Effects of the Noxious Aquatic Weed. Letters in Applied NanoBioScience, 14(3), (2025). https://doi.org/10.33263/LIANBS143.141

[13] S.G. Firisa, G.G. Muleta, A.A. Yimer, Synthesis of nickel oxide nanoparticles and copper-doped nickel oxide nanocomposites using phytolacca dodecandra L'herit leaf extract and evaluation of its antioxidant and photocatalytic activities. ACS omega, 7(49), (2022) 44720. https://doi.org/10.1021/acsomega.2c04042

[14] A. Nashim, S. Pany, K. Parida, Effect of synthesis methods on the activity of NiO/Co_3O_4 as an electrode material for supercapacitor: in the light of X-ray diffraction study. RSC advances, 14(1), (2024) 233-244. https://doi.org/10.1039/d3ra05200a

[15] S.A. Khan, S. Shahid, A. Ayaz, J. Alkahtani, M.S. Elshikh, T. Riaz, Phytomolecules-coated NiO nanoparticles synthesis using abutilon indicum leaf extract: antioxidant, antibacterial, and anticancer activities. International Journal of Nanomedicine, (2021) 1757-1773. https://doi.org/10.2147/IJN.S294012

[16] A. Singh, V. Goyal, J. Singh, H. Kaur, S. Kumar, K.M. Batoo, J. Gaur, M. Pal, M. Rawat, S. Hussain, Structurally and morphologically

engineered single-pot biogenic synthesis of NiO nanoparticles with enhanced photocatalytic and antimicrobial activities. Journal of Cleaner Production, 343, (2022) 131026. https://doi.org/10.1016/j.jclepro.2022.131026

[17] Y. Singh, R.S. Sodhi, P.P. Singh, S. Kaushal, Biosynthesis of NiO nanoparticles using Spirogyra sp. cell-free extract and their potential biological applications. Materials Advances, 3(12), (2022) 4991-5000. https://doi.org/10.1039/d2ma00114d

[18] L. Suresh, R. Snega, P.G. Sravanthy, M. Saravanan, Phytosynthesis of Nickel Oxide Nanoparticles and Their Antioxidant and Antibacterial Efficacy Studies. Cureus, 16(4), (2024) e58064. https://doi.org/10.7759/cureus.58064

[19] K. Varunkumar, R. Hussain, G. Hegde, A.S. Ethiraj, Effect of calcination temperature on Cu doped NiO nanoparticles prepared via wet-chemical method: structural, optical and morphological studies. Materials science in semiconductor processing, 66, (2017) 149-156. https://doi.org/10.1016/j.mssp.2017.04.009

[20] O. El-Atwani, H. Kim, C. Harvey, M. Efe, S.A. Maloy, Limitations of thermal stability analysis via in-situ TEM/heating experiments. Nanomaterials, 11(10), (2021) 2541. https://doi.org/10.3390/nano11102541

[21] A. Malysa, J. Wezgowiec, S. Orzeszek, W. Florjanski, M. Zietek, M. Wieckiewicz, Effect of different surface treatment methods on bond strength of dental ceramics to dental hard tissues: A systematic review. Molecules, 26(5), (2021) 1223. https://doi.org/10.3390/molecules26051223

[22] A.C. Gandhi, S.Y. Wu, Strong Deep-Level-Emission Photoluminescence in Nio Nanoparticles. Nanomaterials, 7(8), (2017) 231. https://doi.org/10.3390/nano7080231

[23] D. Maarisetty, S.S. Baral, Effect of defects on optical, electronic, and interface properties of NiO/SnO_2 heterostructures: dual-functional solar photocatalytic H_2 production and RhB degradation. ACS applied materials & interfaces, 13(50), (2021) 60002-60017. https://doi.org/10.1021/acsami.1c19544

[24] S. Prabhu, T. Daniel Thangadurai, P. Vijai Bharathy, Pon Kalugasalam. Synthesis and characterization of nickel oxide nanoparticles using Clitoria ternatea flower extract: Photocatalytic dye degradation under sunlight and antibacterial activity applications. Results in Chemistry, 4, (2022) 100285. https://doi.org/10.1016/j.rechem.2022.100285

[25] J. Sukumaran, M. Priya, R. Venkatesan, K. Sathiasivan, M.R. Khan, S.C. Kim, Green Synthesis of Nickel Oxide Nanoparticles Using Leaf Extract of Aegle marmelos and Their Antibacterial, Anti-Oxidant, and In Vitro Cytotoxicity Activity. Microscopy Research and Technique, 88(10), (2025) 2830-2842. https://doi.org/10.1002/jemt.70054

[26] H.F. Etefa, D.J. Nemera, F.B. Dejene, Green synthesis of nickel oxide NPs incorporating carbon dots for antimicrobial activities. ACS omega, 8(41), (2023) 38418-38425. https://doi.org/10.1021/acsomega.3c05204

[27] O.A. Zelekew, P.A. Fufa, F.K. Sabir, A.D. Duma, Water hyacinth plant extract mediated green synthesis of Cr_2O_3/ZnO composite photocatalyst for the degradation of organic dye. Heliyon, 7(7), (2021). https://doi.org/10.1016/j.heliyon.2021.e07652

[28] F. Moradnia, S.T. Fardood, A. Zarei, S. Heidarzadeh, A. Ramazani, Green synthesis of nickel oxide nanoparticles using plant extracts: an overview of their antibacterial, catalytic, and photocatalytic efficiency in the degradation of organic pollutants. Iranian Journal of Catalysis, 14(1), (2024). https://doi.org/10.57647/j.ijc.2024.1401.01

[29] V. Lakshmikanth Reddy, S. Lakshmikanth, Synthesis of NiO nanoparticles prepared via a green process using Azadirachta indica, Morinda citrifolia, and Terminalia elliptica for biological applications. BioNanoScience, 13(3) (2023) 1184-1196. https://doi.org/10.1007/s12668-023-01145-7

[30] A. Sani, D. Hassan, A.T. Khalil, A. Mughal, A. El-Mallul, M. Ayaz, Z.K. Shinwari, M. Maaza, Floral extracts-mediated green synthesis of NiO nanoparticles and their diverse pharmacological evaluations. Journal of Biomolecular Structure and Dynamics, 39(11), (2021) 4133-4147. https://doi.org/10.1080/07391102.2020.1775120

[31] S. Vivekanandhan, Combustion process using plant-based fuels for the synthesis of metal-oxide nanostructures. ChemistrySelect, 4(27), (2019) 8026-8042. https://doi.org/10.1002/slct.201900103

[32] D.J. Pochapski, C. Carvalho dos Santos, G.W. Leite, S.H Pulcinelli, C.V. Santilli, Zeta potential and colloidal stability predictions for inorganic nanoparticle dispersions: effects of experimental conditions and electrokinetic models on the interpretation of results. Langmuir, 37(45), (2021) 13379-13389. https://doi.org/10.1021/acs.langmuir.1c02056

[33] A.E. Ferenji, Y.E. Hassen, S.L. Mekuria, W.M. Girma, Biogenic mediated green synthesis of NiO

nanoparticles for adsorptive removal of lead from aqueous solution. Heliyon, 10(11), (2024). https://doi.org/10.1016/j.heliyon.2024.e31669

[34] M. Danish, J. Ahmad, P. Muhammad, S. Javed, A. Saeed, N. Khaliq, M.H. Bhatti, R. Ghazi, A.F. Kiyani, H. Ullah, Y. Xie, G. Ali, Anodic NiO nanoparticles as high-performance asymmetric supercapacitor devices in hybrid electrolytes. RSC advances, 15(53), (2025) 45665-45677. https://doi.org/10.1039/d5ra07019h

Authors Contribution Statement

K. Leninbarathi: Conceptualization, Methodology, Investigation, Data curation, Formal analysis, Visualization, Writing – original draft, Writing – review & editing. O. Anand: Investigation, Methodology, Data curation, Formal analysis, Writing – review & editing. S. Sathiyaraj: Investigation, Validation, Formal analysis, Writing – review & editing. Aysha E. Shamaki: Data analysis, Validation, Visualization, Writing – review & editing. Alaa F. Abd El-Rehim: Formal analysis, Validation, Interpretation of results, Writing – review & editing. Ch. Srinivas: Methodology, Characterization analysis, Validation, Writing – review & editing. Vinayakprasanna N. Hegde: Formal analysis, Visualization, Validation, Writing – review & editing. R.T. Karunakaran: Conceptualization, Supervision, Project administration, Validation, Writing – review & editing. All authors reviewed and approved the final version of the manuscript and agreed to be accountable for the integrity and accuracy of the work.

Acknowledgment

The authors extend their appreciation to the Academic Innovation Leadership Program under King Khalid University Developmental Project for Stimulating Sustainable Innovation Ecosystems toward Future Manufacturing through the project code VPGSR/FM/PG52.

Competing Interests

The authors declare that there are no conflicts of interest regarding the publication of this manuscript.

Data Availability

The data supporting the findings of this study can be obtained from the corresponding author upon reasonable request.

Has this article screened for similarity?

Yes

About the License